Three-Dimensional Stretched Boundary Layer Flow of Casson Nanofluid in Rotating Frame with Bio-convection Phenomenon

Muhammad Sohail[1,*], Syed Qasim Hussain Shah[1], Faisal Sultan[1], Shah Jahan[1] and Syed Tehseen Abbas[1]

[1]Institute of Mathematics, Khwaja Fareed University of Engineering & Information Technology, Rahim Yar Khan 64200, Pakistan

Corresponding author: muhammad_sohail111@yahoo.com;

Abstract: This paper describes the three-dimensional Casson nanofluid's rotating flow with bioconvection Phenomenon containing microorganisms, thermal radiation, and magnetic effects. This research has real-world applications in a variety of processes, including oceanography, crystal growth, computer storage devices, lubrication, and rotating machinery. The present model incorporates the Buongiorno nanofluid model, which describes the Brownian and thermophoresis motion of nanoparticles. The boundaries layer approximation and non-Newtonian three-dimensional Casson fluid model are encompassed in the modelling of the nonlinear partial differential system. Finding an analytical clarification to the 3D Casson nanofluid flow past a rotating frame involving bio-convection phenomenon nonlinear differential equation is the goal of this task. Graphical results are obtained using the OHAM. The effects of different numbers are examined with respect to velocities, thermal field, magnetic field, nanoparticle concentration, and microorganism field. The temperature distribution is lessened with a greater Prandtl number. The temperature and solute field of a species increases with an upsurge in the estimation of the thermophoresis parameter. The microorganism's field decreases when the Peclet parameter, bioconvection Lewis number, and Microorganisms difference number increase.

Keywords: Casson fluid; 3D flow; MHD; Nanofluid; OHAM; Rotating Frame; Stretching Sheet; Buongiorno model; Bio-convection.

1. Introduction

Nanofluids are used in engineering branches, like mechanical engineering, chemical engineering, power engineering, agricultural engineering, refrigerators, aero planes, and vehicles. The use of nanofluid has increased oil recovery (EOR) in saltwater environments. Choi and Eastman [1] have presentation the original study that popularized the idea of nanofluids. Nayak

et al. [2] report nanofluid convective flow involving chemical reaction across an exponentially extending sheet. Shehzad et al. [3] explored the Casson nanofluid models. Sajid and Ali [4] provide a critical study of recent advancements in the use of nanofluid in heat transfer devices. Chaakraborty and Panigrahi [5] explored the stability of nanofluid. The use of convective boundary conditions, Nadeem et al. [6] examined Casson nanofluid flow across a linear stretched sheet within a three-dimensional Magnetohydrodynamic boundary layer. Convective boundary conditions were employed by Sulochana et al. [7] to investigate 3D Casson nanofluid flow on a stretched sheet. Heat transfer with slip, convective boundary conditions, and MHD stagnating point flow were employed by Ibrahim and Makinde [8] to investigate the Casson nanofluid flow across a stretched sheet. Santoshi et al. [9] analyzed Casson-Carreau nanofluids numerically in three dimensions. Kumaran and Sandeep [10] examined Casson fluid flow while taking into account Brownian motion. Archana et al. [11] tested Casson nanofluid is used as a lubricant. The Shaheen et al. [12] was studied Dufour-sort effect with Casson nanofluid in three-dimensional containing dust particles and changing characteristics in a permeable medium. An excellent case study for researching the Casson nanofluid instabilities of material across a stretched sheet, as investigated. Under thermal radiation, Jamshed et al. [13] carried out an excellent case study with an unstable Casson nanofluid assessment across a stretched sheet.

Many industrial applications involved in rotating frame systems. Whether a vortex formed or a little motion was created, the issue of spinning fluids was inevitably brought up. The current experiment concentrated on how rotating frame systems affected the flow. Rotating frame flow is frequently used in the broad range of industries, including the design of turbines, cheerleaders, processing of food, engine, gearing, brake parts, disc cleaners, medical devices, viscometers, distinctive rotating geometry for internal air conditioning, compressors, and cyclone separators. Wang [14] sought to comprehend rotational flow over-stretching geometries at first and finally acquired the required results using the perturbation approach. Rotating flow in three-dimension with suction over a sheet that is diminishing exponentially explored by Rosali et al. [15]. Radha et al. [16] analyzed Casson nanofluid motion in three dimensions using a stretched sheet. For MHD radiative Casson nanofluid flow using a moving disc saturated in a porous medium. Noranuar et al. [17] has studied dual diffusing in non-coaxial rotating frame. Mohamed G. Ibrahim et al. [18] conducted semi-numerical computations to examine the rotating Casson nanofluid flow with Arrhenius energy effects and velocity slip possessions under convective

conditions. Raju and Sandeep [19] have investigated the ferrous nanoparticles were suspended in a Casson nanofluid in a rotating frame above a rotating cone. Khan et al. [20] study utilized Buongiorno's model to carry out a computational assessment of nanofluid heat and flow transmission across a rotating frame. Analytical methodologies for the 3D investigation of condensing nanofluid layers on an angled rotating frame were discussed by Hatami et al. [21]. A rotating flow's Casson nanofluid's reaction to nonlinear thermal radiation Arcana et al. [22] inspected. Nanofluids in an orbiting frame were the subject of a Darcy-Forchheimer flow deliberate by Hayat et al. [23]. Rashid et al. [24] examine how Darcy-Forchheimer operates within a porous material in order to evaluate the velocity field in rotating frame examinations. Ali et al. [25] finite element analysis used the thermal flux modal to examine how the MHD affects a Casson nanofluid's rotating flow. Carbon nanotubes in an MHD Casson nanofluid move non-coaxially past a rotating frame with the porosity effects addressed by Noranuar et al. [26]. In three dimensions, Aziz et al. [27] scrutinized the numerical modelling of a spinning nanofluid with entropy production. Aziz et al. [28] looked at the entropy analysis of the Powell-Eyring hybrid nanofluid while taking viscous dissipation and linear thermal radiation into consideration. To investigate the theoretical framework of Cattaneo-Christov thermal flux consequences on Williamson hybrid nanofluids based on engine oil, Jamshed et al. [29] conducted a thermal case study. Jamshed and Aziz [30] explored the effects of variable thermal conductivity, numerous nanoparticle shapes, and thermal radiation on the Fe3O4/methanol Powell-Eyring nanofluid and Cu within solar thermal accumulators using a comparative entropy-based methodology. Jamshed et al. [31] scrutinized the fluid flow over an absorbent shrinkable sheet with Ohmic heat resistance utilizing numerical heat and solvent transfer simulation. Sajid et al. [32] introduced this study, which looked at the influence of tetra nanoparticles that are hybrids on binary fluids with ethanol biofuels serving as the base fluid and the catalytic interaction, Crosser model, and novel Hamilton. Kai et al. [33] conducted a scrutiny on the stimulus of applied restricted magnetic fields on the Ag-TiO_2 hybrid fluid flow within an enclosure that is induced by numerous magnetic sources. Hanif et al. [34] conducted a numerical Crank-Nicolson methodology investigation on the hybridity of an aluminum alloy nanofluid that was flowing through a stretchy horizontal plate and had a thermal resistive effect. Kai et al. [35] inspected the temperature and created vortices in a hybridized nanofluid that was flowing in an implicit solution in two different directions. According to Akolade and Tijani [36], there are

nonlinear radiation effects when it comes to how different transport parameters affect the magnetized 3D flow of the Casson nanofluid across a Riga plate.

Stretching sheet usually refers to a theoretical model that is used to investigate how a nanofluid flows and transfers heat along a stretching surface. A stretched sheet's orientation was the focus of the heat transfer and stagnation-point flows in a Casson fluid were discovered by Mustafa et al. [37]. The idea for a 3D Casson nanofluid that is flow across a porous sheet that is linearly expanding was created by Nadeem et al. [38]. Using a linear stretched sheet, Mahanta and Shaw [39] discussed the Casson fluid flow. Oyelakin et al. [40] expressed an unsteady Casson nanofluid that flows onto a sheet that was stretched with conditions including heat radiation and convection. Shah [41] investigates thermophoresis's impact on a 3D non-Newtonian nanofluid with continuous current, related to the Hall effects in a Brownian motion rotating frame. Research on the effects of diffusing on the hydrodynamics Anwar et al. [42] looks at how the Casson nanofluid boundary zone moves across a stretched surface. Considering viscous dissipation, a viscous Casson fluid can be injected and sucked via a stretched surface by Hussanan et al. [43]. Melting affects radiation-induced magnetohydrodynamic Casson nanofluid motion via a stretched sheet via a porous media, as demonstrated by Mabood and Das [44]. Ullah et al. [45] investigated a Williamson-dusty nanoliquid flow across a stretched plate using MHD mixed convection. Using Cattaneo-Christov theory, Khan et al. [46] surveyed the stratification consequence brought on by an exponentially stretched sheet in a rotating frame beneath the inspiration of a magnetic field as well as heat transfer analysis of Casson fluid flow. 3D Casson nanofluid flow was inspected by Lone et al. [47] on a bidirectional linear stretchy sheet that was home to gyrotactic microorganisms. Shah et al. [48] examine the Casson ferrofluid on a stretched sheet utilizing the efficient thermal conductivity model. With the use of an MHD Casson nanofluid, Gangaiah et al. [49] examined how heat radiation impacts mixed convection flow across an exponentially increasing sheet. Using the Keller box as a Buongiorno model, Rafique et al. [50] examined a three-dimensional Casson nanofluid study on an inclined surface that combined Brownian and thermophoretic dispersion. Ragupathi et al. [51] have studied 3D Casson nanofluid flow with exponential thermal effects and Arrhenius activation energy on a stretched sheet. Puneeth et al. [52] have premeditated a 3D hybrid Casson nanofluid flow that crosses a non-linear stretching surface. According to Al-Mamun et al. [53], a permeable stretching sheet was utilized to replicate periodic MHD Casson nanofluid flow. Gangadhar et al.

[54] investigation of the Casson flows through a stretched sheet. In 2006, R. Buongiorno expanded the conventional single-phase fluid model and proposed the Buongiorno model to account for the inclusion of nanoparticle in a base fluid. Garoosi et al. [55] research suggests that the Buongiorno model might mimic the nanofluid's natural convection in heat exchangers. Buongiorno nanofluid concept impacts on optical heat and mass transmission have been demonstrated by Turkyilmazoglu [56]. 3D MHD viscous flow with thermal radiation and dissipation of viscous fluid is examine by Akbar and Sohail [57]. Li et al. [58] explored the under slip circumstances effects of buoyancy and dissipation of viscous on a 3D magnetohydrodynamic viscous hybrids nano fluid (MgO-TiO_2). Nazir et al. [59] investigated the use of mesh-free studies and the FE approach in a non-Fourier way to investigate uses for changeable thermal features in Carreau materials including ion hall and slide forces towards cone. A monophasic-magnetized nanofluid with Ohmic heating and a thermal hop was studied for its entropy and heating case specification by Zhang et al. [60] using finite element techniques. To investigate second-grade nanofluid flow's radiative heat exchange via a porous flat surface, Jamshed et al. [61] employed a one-phase mathematical model. To analyze the flow of an Ag-Cu/EO hybrid Williamson nanofluid across a stretched surface with an outline factor, Jamshed et al. [62] performed single-phase research. The Casson nanofluid generated by an unstable stretching surface was premeditated by Ahmad et al. [63] using features of chemical reaction and heat radiation in magnetohydrodynamic time-dependent three-dimensional simulations. A second-class fluid with varying thermal conductivity was studied by Haider et al. [64] in terms of the transfer of energy dependent on time Cattaneo-Christov double diffusion. Employing the spectral relaxation technique, Rasool et al. [65] have studied the bioconvection and chemical reactions for an elevated influenced Cross nanofluid over a persuaded cylinder. The Casson nano-fluid stream over a plate was premeditated by Farooq et al. [66] using a variety of techniques, such as bioconvection, exponential heat sources, and motile microorganisms. Within magnetohydrodynamics, bioconvection Naidu et al. [67] planned the Casson nanofluid, which is made up of motile microorganisms using convective boundary conditions. The study's findings have significant ramifications for biological and technical systems, including the petroleum industry, bio-microsystems, designing bio-cells, biomedicine, and other fields which microorganisms and nanoparticles are crucial to improving energy conservation efficiency. Tawade et al. [68] looked into the issue of continual laminar flow of a nanofluid across a barrier

layer utilizing Cassona heat transfer via a linearly increasing sheet. Variable heat conductivity and a Lorentz force were employed by Botmart et al. [69] in their mathematical formulation of the cross model to study the nanoscale thermal transmission phenomena of fluids. The current study advances the numerical treatment relating a mix of convective inclination magnetized Cross nanofluid with changing heat conductivity across a moving permeable surface, based on variable viscosity, as studied by Darvesh et al. [70]. Al-Kouz and Owhaib [71] conducted a numerical study utilizing a three-dimensional Casson's nanofluid that was flowing via a rotating frame and subjected to viscous warming and calculated heat flux.

The Optimal Homotopy analytical approach is used for bio-convective Casson model to produce graphical findings. The impacts of various parameters are investigated in relation to temperature field, nanoparticle concentration, microbiological field, and velocities. The temperature distribution is lessened with a greater Prandtl number. As the thermophoresis parameter is estimated more, the specie's solute zone and heat grow. The microorganism's field shrinkages with increasing ethics of the bioconvection Lewis number, Peclet parameter, and microorganism's difference value.

2. Problem Formulation

We examine the extended non-Newtonian Casson nanofluid's three-dimensional laminar flow. The fluid space is regarded as being at $z \geq 0$. A constant rate of rotation ω about the z-axis is experienced by the incompressible Casson nanofluid. Fig. 1 depicts a schematic illustration of the problem being studied.

The present problem under investigation governing equations are defined below, see reference [71].

$$\frac{\partial u}{\partial x}+\frac{\partial v}{\partial y}+\frac{\partial w}{\partial z}=0, \tag{1}$$

$$\rho\left(u\frac{\partial u}{\partial x}+v\frac{\partial u}{\partial y}+w\frac{\partial u}{\partial z}-2\omega v\right)=\mu\left(1+\frac{1}{\beta}\right)\frac{\partial^2 u}{\partial z^2}-\sigma B_0^2 u, \tag{2}$$

$$\rho\left(u\frac{\partial v}{\partial x}+v\frac{\partial v}{\partial y}+w\frac{\partial v}{\partial z}+2\omega u\right)=\mu\left(1+\frac{1}{\beta}\right)\frac{\partial^2 v}{\partial z^2}-\sigma B_0^2 v, \tag{3}$$

$$\rho C_p\left(u\frac{\partial T}{\partial x}+v\frac{\partial T}{\partial y}+w\frac{\partial T}{\partial z}\right)=k\left(\frac{\partial^2 T}{\partial z^2}\right)+\mu\left(1+\frac{1}{\beta}\right)\left(\left(\frac{\partial u}{\partial z}\right)^2+\left(\frac{\partial v}{\partial z}\right)^2\right)$$
$$+\left(\rho C_p\right)_{np}\left\{D_B\left(\frac{\partial T}{\partial z}\right)\left(\frac{\partial C}{\partial z}\right)+\frac{D_T}{T_\infty}\left(\frac{\partial T}{\partial z}\right)^2\right\}, \tag{4}$$

$$u\frac{\partial C}{\partial x}+v\frac{\partial C}{\partial y}+w\frac{\partial C}{\partial z}=D_B\frac{\partial^2 C}{\partial z^2}+\frac{D_T}{T_\infty}\frac{\partial^2 T}{\partial z^2} \tag{5}$$

$$u\frac{\partial n}{\partial x}+v\frac{\partial n}{\partial y}+w\frac{\partial n}{\partial z}+\frac{bW_c}{\left(C_W-C_\infty\right)}\left[\frac{\partial}{\partial Z}\left(n\frac{\partial C}{\partial z}\right)\right]=D_m\left(\frac{\partial^2 n}{\partial z^2}\right). \tag{6}$$

When the appropriate boundary conditions are

$$u=u_w(x)=ax,\ v=v_w(y)=by,\ w=w,\ C=C_w,\ T=T_w,\ n=n_w,\text{ as } z=0,$$

$$u\to 0,\ v\to 0,\ w\to 0,\ C\to C_\infty,\ T\to T_\infty,\ n\to n_\infty,\text{ when } z\to\infty. \tag{7}$$

With transformation

$$u=axf'(\eta),\ v=ayg'(\eta),\ w=-\sqrt{av}\left(f(\eta)+g(\eta)\right),\ \eta=z\sqrt{\frac{a}{\nu}},$$

$$n=\left(n_w-n_\infty\right)n(\eta)+n_\infty,\ C=\left(C_w-C_\infty\right)\varphi(\eta)+C_\infty,\ T=\left(T_w-T_\infty\right)\theta(\eta)+T_\infty. \tag{8}$$

The non-dimensional ODEs are obtained by using equations (7-8) in equations (2-5)

$$\left(1+\frac{1}{\beta}\right)f'''+\left(f+g\right)f''-\left(f'\right)^2+2Rog'-M^2f'=0, \tag{9}$$

$$\left(1+\frac{1}{\beta}\right)g'''+(f+g)g''-(g')^2-2Rof'-M^2g'=0, \tag{10}$$

$$\frac{1}{P_r}\theta''+(f+g)\theta'+Nt(\theta')^2+Nb\theta'\varphi'+Ec\left((f'')^2+(g'')^2\right)\left(1+\frac{1}{\beta}\right)=0, \tag{11}$$

$$\varphi''\frac{Nt}{Nb}\theta''+Le(f+g)\varphi'=0, \tag{12}$$

$$\chi''+Lb(f+g)\chi'-Pe\left[(\chi+\delta_1)\varphi''+\chi'\varphi'\right]=0. \tag{13}$$

The problems transformed boundary conditions

$$f(0)=S,\ f'(0)=1,\ g(0)=0,\ g'(0)=\alpha,\ \theta(0)=1,\ \chi(0)=1 \text{ when } z\to 0,$$

$$f'(\infty)=0,\ g'(\infty)=0,\ \theta(\infty)=0,\ \varphi(\infty)=0,\ \chi(\infty)=0 \text{ when } z\to\infty. \tag{14}$$

The values that occurred as the coefficient of f,θ,φ are known as several physical parameters that impact the issue models during the non-dimensionalities process:

$$Ro=\frac{\omega}{a},\ S_c=\frac{\nu}{D_B},\ Ec=\frac{u_w^2}{C_p(T_w-T_\infty)},\ Lb=\frac{\nu}{D_m},\ Pe=\frac{bW_c}{D_m},\ M=\frac{\sigma B_0^2}{\rho a},$$

$$Nb=\frac{(\rho C_p)_{np}D_B(C_w-C_\infty)}{\rho C_p C_\infty \nu},\ Nt=\frac{(\rho C_p)_{np}D_T(T_w-T_\infty)}{\rho C_p T_\infty \nu},\ \delta_1=\frac{n_\infty}{T_w-T_\infty}. \tag{15}$$

This study's quantities of practical significance are the Sherwood number Sh_x, the Nusselt number Nu_x, and skin friction coefficients which are respectively defined as

$$Sf_x=\frac{\tau_{wx}}{\rho u_w^2},\quad \tau_{wx}=\mu\left[\left(1+\frac{1}{\beta}\right)\frac{\partial u}{\partial z}\right]_{z=0},\quad Sf_y=\frac{\tau_{wy}}{\rho u_w^2},\quad \tau_{wy}=\mu\left[\left(1+\frac{1}{\beta}\right)\frac{\partial v}{\partial z}\right]_{z=0},$$

$$Nu_x = \frac{xq_w}{k\left(T_w - T_\infty\right)},\ q_w = \left[-k\frac{\partial T}{\partial z}\right]_{z=0},\ Sh_x = \frac{xq_m}{k\left(C_w - C_\infty\right)},\ q_m = \left[-k\frac{\partial C}{\partial z}\right]_{z=0}.$$

The following are non-dimensional expressions for drag forces (skin friction), thermal rate of flow (Nusselt number), and mass rate for flux (Sherwood number)

$$\mathrm{Re}_x^{0.5}\, Sf_x = \left(1+\frac{1}{\beta}\right) f''(0), \tag{16}$$

$$\mathrm{Re}_y^{0.5}\, Sf_y = \left(1+\frac{1}{\beta}\right) g''(0), \tag{17}$$

$$\mathrm{Re}_x^{-0.5}\, Nu_x = -\theta'(0), \tag{18}$$

$$\mathrm{Re}_x^{-0.5}\, Sh_x = -\varphi'(0). \tag{19}$$

Where $\mathrm{Re}_x = \frac{u_w x}{\nu}$ is Reynolds number.

3. Methodology

The nonlinear BVP Equations (9) to (13) are analytically solved, and graphical results are generated utilizing the Homotopy Analytical Method (HAM) BVPh2.0 as explained through Fig. 2. These are following the initial estimates and auxiliary linear operators:

$$f_0(\eta) = 1 - \frac{1}{\tilde{e}xp(\eta)} + S,\ g_0(\eta) = \alpha\left(1 - \frac{1}{\tilde{e}xp(\eta)}\right),\ \theta_0(\eta) = \frac{1}{\tilde{e}xp(\eta)},$$
$$\varphi_0(\eta) = \frac{1}{\tilde{e}xp(\eta)},\ \chi_0(\eta) = \frac{1}{\tilde{e}xp(\eta)}, \tag{20}$$

$$G_f = f''' - f',\ G_g = g''' - g',\ G_\theta = \theta'' - \theta',\ G_\varphi = \varphi'' - \varphi',\ G_\chi = \chi'' - \chi'. \tag{21}$$

By

$$G_f\left[F_1+F_2e^{\eta}+F_3e^{-\eta}\right]=0,$$

$$G_g\left[F_4+F_5e^{\eta}+F_6e^{-\eta}\right]=0,$$

$$G_\theta\left[F_7e^{\eta}+F_8e^{-\eta}\right]=0,$$

$$G_\varphi\left[F_9e^{\eta}+F_{10}e^{-\eta}\right]=0, \qquad (22)$$

$$G_\chi\left[F_{11}e^{\eta}+F_{12}e^{-\eta}\right]=0.$$

4. Results and Discussion

We study the rotational flow of a three-dimensional Casson nanofluid with heat radiation, magnetic effects, and a bioconvection phenomenon including microorganisms. This study's analytical solution is shown in Figs. 3, 4, 5, 6, 7, 8, 9, 10, 11, 12, 13, 14, 15, 16, 17, 18 and 19. Fig. 3 shows the when β levels are raised, the axial velocity is decreased, then magnitude of axial velocity is deceased. Fig. 4 shows the higher rotation factor values denote a lower axial velocity rate, greater values of Ro therefore result in a decrease in the axial velocity's magnitude. As the M rises, the axial velocity profile shrinkages, as seen in Fig. 5. Both the particle nanofluid and carrier-based fluid have their velocity reduced by the magnetic field. Fig. 6 shows how the transverse velocities $g'(\eta)$ increases in magnitude as β rises. Fig. 7 shows the magnitude for the transverse velocities $g'(\eta)$ growing as Ro increases. The longitudinal velocity profile rises as the M upsurges, as seen in Fig. 8. The velocity of the particle nanofluid and the carrier-based fluid both increase in the existence of a magnetic field. As the Prandtl number surges, Fig. 9 shows how the ambient temperature profile decreases and the nanofluid's thermal conductivity shrinkages. Fig. 10 shows the stimulus of the Brownian parameter that is physically linked to the expected velocity of collisions and nanoparticles. Fig. 11 illustrates the temperature profile rises with higher Nt values and the nanofluid produces more heat. The increasing values of Ec in Fig. 12 demonstrate the layer structure's tendency to rise with temperature. The rising Casson fluid parameter values and the layer structure's propensity to

contract with temperature are depicted in Fig. 13. As can be seen in Fig. 14, the concentration profile rises as the thermophoresis parameter is raised. A rise in the thermophoresis parameter grades in a growth in the concentration boundary layer thickness. As can be shown in Fig. 15, the concentration of nanoparticles increases with an upturn in the Brownian parameter Nb. Fig. 16 depicts the reduced concentration of nanoparticles layer structure induced by lower mass diffusivity due to higher Le values. Fig. 17 illustrates both factors have a markedly reducing influence on $\chi(\eta)$ due to the reduction in diffusion of the motile density of the bacterium caused by Lb. Fig. 18 shows the rise in the value of the Peclet number Pe induces a rise in the diffusivity of the microbe, and therefore the microorganism concentration function $\chi(\eta)$ decreases. Fig. 19 shows the accumulative value of the microorganism concentration difference number δ_1 reduces the microorganism concentration function $\chi(\eta)$. Increasing the values of Casson fluid parameters β marks in a drop in the Nusselt numbers, Sherwood number, and skin friction, as table 1 illustrates.

5. Conclusion

The rotational flow of a 3D Casson nanofluid comprising microorganisms, heat radiation, and magnetic influences is studied. The following summarizes the main findings of the current research:

- A similar behavior is observed when increasing or decreasing the magnetic field or the caisson fluid profile;
- The increase in heat and solute thickness of layers is caused by the thermo-diffusion caused by nanoparticles;
- When both Nb and Nt are adjusted to greater levels, the heat transfer rate at the frame achieves its maximum. This suggests that raising the Nusselt number values centrals to an increased heat transfer rate at the frame;
- The concentration of nanoparticles decreases as the microbe concentration and Lewis value both increase;

- Increasing the changes of the Lewis number of bioconvection Lb, Peclet number Pe, and the microorganisms variance number δ_1 results in a decrease of the motile microorganisms density field $\chi(\eta)$.

Abbreviation	Full Name
β	Dimensionless Casson fluid factor
C_w	Plate nanoparticles concentration
C_p	Specific heat
D_B	Brownian diffusion factor
D_T	Thermophoresis diffusion factor
Ec	Eckert number
k	Heat conductivity
Le	Lewis Coefficient
Nb	Factor of Brownian motion
Nt	Factor of Thermophoresis
P_r	Prandtl coefficient
Re	Reynolds coefficient
Ro	Rotation parameter
T_w	Temperature of fluid
T_∞	Temperature of ambient

φ	Dimensionless nanoparticle concentration
ρC_p	Casson nanofluid heat capacity
$\left(\rho C_p\right)_{np}$	Nanoparticles heat capacity
A	Thermal diffusivity $\left(\frac{m^2}{s}\right)$
Np	Nanoparticles
Pe	Peclet Number
M	Magnetic Parameter
W_c	Maximum cell Swimming Speed
D_m	Microorganism Coefficient
Lb	Concentration of microorganisms
B_0	Magnetic Field
δ_1	microorganisms difference number
χ	density field of motile microorganisms

References

1. Choi, S. U., & Eastman, J. A. "Enhancing thermal conductivity of fluids with nanoparticles", (No. ANL/MSD/CP-84938; CONF-951135-29). *Argonne National Lab. (ANL), Argonne, IL (United States)*, pp. (1995).

2. Nayak, M. K., Akbar, N. S., Tripathi, D., et al. "MHD 3D free convective flow of nanofluid over an exponentially stretching sheet with chemical reaction", *Advanced Powder Technology*, **28**(9), pp. 2159-2166 (2017). https://doi.org/10.1016/j.apt.2017.05.022
3. Shehzad, S. A., Hayat, T., & Alsaedi, A. "MHD flow of a Casson fluid with power law heat flux and heat source", *Computational and Applied Mathematics*, **37**, pp. 2932-2942 (2018). https://doi.org/10.1007/s40314-017-0492-3
4. Sajid, M. U., & Ali, H. M. "Recent advances in application of nanofluids in heat transfer devices: a critical review", *Renewable and Sustainable Energy Reviews*, **103**, pp. 556-592 (2019). https://doi.org/10.1016/j.rser.2018.12.057
5. Chakraborty, S., & Panigrahi, P. K. "Stability of nanofluid": A review. *Applied Thermal Engineering*, **174**, pp. 115259 (2020). https://doi.org/10.1016/j.applthermaleng.2020.115259
6. Nadeem, S., Haq, R. U., & Akbar, N. S. "MHD three-dimensional boundary layer flow of Casson nanofluid past a linearly stretching sheet with convective boundary condition", *IEEE Transactions on Nanotechnology*, **13**(1), pp. 109-115 (2013). 10.1109/TNANO.2013.2293735
7. Sulochana, C., Ashwinkumar, G. P., & Sandeep, N. "Similarity solution of 3D Casson nanofluid flow over a stretching sheet with convective boundary conditions", *Journal of the Nigerian Mathematical Society*, **35**(1), pp. 128-141 (2016). https://doi.org/10.1016/j.jnnms.2016.01.001
8. Ibrahim, W., & Makinde, O. D. "Magnetohydrodynamic stagnation point flow and heat transfer of Casson nanofluid past a stretching sheet with slip and convective boundary condition", *Journal of Aerospace Engineering*, **29**(2), pp. 04015037 (2016). https://doi.org/10.1061/(ASCE)AS.1943-5525.0000529
9. Naga Santoshi, P., Ramana Reddy, G. V., & Padma, P. "Numerical scrutinization of three dimensional Casson-Carreau nano fluid flow", *Journal of Applied and Computational Mechanics*, **6**(3), pp. 531-542 (2020). 10.22055/JACM.2019.29377.1593
10. Kumaran, G., & Sandeep, N. "Thermophoresis and Brownian moment effects on parabolic flow of MHD Casson and Williamson fluids with cross

diffusion", *Journal of Molecular Liquids*, **233**, pp. 262-269 (2017). https://doi.org/10.1016/j.molliq.2017.03.031

11. Archana, M., Praveena, M. M., Kumar, K. G., et al. "Unsteady squeezed Casson nanofluid flow by considering the slip condition and time- dependent magnetic field", *Heat transfer*, **49**(8), pp. 4907-4922 (2020). https://doi.org/10.1002/htj.21859

12. Shaheen, N., Ramzan, M., Alshehri, A., et al. "Soret–Dufour impact on a three-dimensional Casson nanofluid flow with dust particles and variable characteristics in a permeable media", *Scientific Reports*, **11**(1), pp. 14513 (2021). https://doi.org/10.1038/s41598-021-93797-2

13. Jamshed, W., Goodarzi, M., Prakash, M., et al. "Evaluating the unsteady Casson nanofluid over a stretching sheet with solar thermal radiation: An optimal case study", *Case Studies in Thermal Engineering*, **26**, pp. 101160 (2021). https://doi.org/10.1016/j.csite.2021.101160

14. Wang, C. Y. "Stretching a surface in a rotating fluid", *Zeitschrift für angewandte Mathematik und Physik ZAMP*, **39**(2), pp. 177-185 (1988). https://doi.org/10.1007/BF00945764

15. Rosali, H., Ishak, A., Nazar, R., et al. "Rotating flow over an exponentially shrinking sheet with suction", *Journal of Molecular Liquids*, **211**, pp. 965-969 (2015). https://doi.org/10.1016/j.molliq.2015.08.026

16. Radha, G., Reddappa, B., Tarakaramu, N., et al. "Three Dimensional Casson nanofluid Flow with Convective Boundary Layer via Stretching Sheet", *Journal of Advanced Zoology*, **44**(S5), pp. 1121-1129 (2023). https://doi.org/10.53555/jaz.v44iS5.1141

17. Noranuar, W. N. N., Mohamad, A. Q., Shafie, S., et al. "Heat and mass transfer in non-coaxial rotation of radiative MHD Casson carbon nanofluid flow past a porous medium", *Data Analytics and Applied Mathematics (DAAM)*, **2**(2), pp. 37-51 (2021). https://doi.org/10.15282/daam.v2i2.6832

18. Ibrahim, M. G., & Fawzy, N. A. "Arrhenius energy effect on the rotating flow of Casson nanofluid with convective conditions and velocity slip effects: Semi-

numerical calculations", *Heat Transfer*, **52**(1), pp. 687-706 (2023). https://doi.org/10.1002/htj.22712

19. Raju, C. S. K., & Sandeep, N. "Unsteady Casson nanofluid flow over a rotating cone in a rotating frame filled with ferrous nanoparticles: a numerical study", *Journal of Magnetism and Magnetic Materials*, **421**, pp. 216-224 (2017). https://doi.org/10.1016/j.jmmm.2016.08.013

20. Khan, J. A., Mustafa, M., Hayat, T., et al. "Numerical study of nanofluid flow and heat transfer over a rotating disk using Buongiorno's model", *International Journal of Numerical Methods for Heat & Fluid Flow*, **27**(1), pp. 221-234 (2017). https://doi.org/10.1108/HFF-08-2015-0328

21. Hatami, M., Jing, D., & Yousif, M. A. "Three-dimensional analysis of condensation nanofluid film on an inclined rotating disk by efficient analytical methods", *Arab Journal of Basic and Applied Sciences*, **25**(1), pp. 28-37 (2018). https://doi.org/10.1080/25765299.2018.1449415

22. Archana, M., Gireesha, B. J., Prasannakumara, B. C., et al. "Influence of nonlinear thermal radiation on rotating flow of Casson nanofluid", *Nonlinear Engineering*, ***7(2)***, pp. 91-101 (2018). https://doi.org/10.1515/nleng-2017-0041

23. Hayat, T., Aziz, A., Muhammad, T., et al. "Darcy-Forchheimer flow of nanofluid in a rotating frame", *International Journal of Numerical Methods for Heat & Fluid Flow*, **28**(12), pp. 2895-2915 (2018). https://doi.org/10.1108/HFF-01-2018-0021

24. Rashid, S., Hayat, T., Qayyum, S., et al. "Three-dimensional rotating Darcy–Forchheimer flow with activation energy", *International Journal of Numerical Methods for Heat & Fluid Flow*, **29**(3), pp. 935-948 (2019). https://doi.org/10.1108/HFF-06-2018-0292

25. Saeed, A., Shah, Z., Islam, S., et al. "Three-dimensional Casson nanofluid thin film flow over an inclined rotating disk with the impact of heat generation/consumption and thermal radiation", *Coatings*, **9**(4), pp. 248 (2019). https://doi.org/10.3390/coatings9040248

26. Noranuar, W. N. I. N., Mohamad, A. Q., Shafie, S., et al. "Non-coaxial rotation flow of MHD Casson nanofluid carbon nanotubes past a moving disk with porosity

effect", *Ain Shams Engineering Journal*, **12**(4), pp. 4099-4110 (2021). https://doi.org/10.1016/j.asej.2021.03.011

27. Aziz, A., Aziz, A., Ullah, I., et al. "Numerical simulation for 3D rotating flow of nanofluid with entropy generation", *International Journal of Modelling and Simulation*, pp. 1-22 (2022). https://doi.org/10.1080/02286203.2022.2051993

28. Aziz, A., Jamshed, W., Aziz, T., et al. "Entropy analysis of Powell–Eyring hybrid nanofluid including effect of linear thermal radiation and viscous dissipation", *Journal of Thermal Analysis and Calorimetry*, **143**, pp. 1331-1343 (2021). https://doi.org/10.1007/s10973-020-10210-2

29. Jamshed, W., Nisar, K. S., Ibrahim, R. W., et al. "Computational frame work of Cattaneo-Christov heat flux effects on Engine Oil based Williamson hybrid nanofluids: A thermal case study", *Case Studies in Thermal Engineering*, **26**, pp. 101179 (2021). https://doi.org/10.1016/j.csite.2021.101179

30. Jamshed, W., & Aziz, A. "A comparative entropy based analysis of Cu and Fe3O4/methanol Powell-Eyring nanofluid in solar thermal collectors subjected to thermal radiation, variable thermal conductivity and impact of different nanoparticles shape", *Results in physics*, **9**, pp. 195-205 (2018). https://doi.org/10.1016/j.rinp.2018.01.063

31. Jamshed, W., Eid, M. R., Rehman, S., et al. "Numerical heat and solutal transfer simulation of fluid flowing via absorptive shrinkable sheet with Ohmic heat resistance", *Numerical Heat Transfer, Part A: Applications*, pp. 1-17 (2023). https://doi.org/10.1080/10407782.2023.2206062

32. Sajid, T., Gari, A. A., Jamshed, W., et al. M. "Case study of autocatalysis reactions on tetra hybrid binary nanofluid flow via Riga wedge: Biofuel thermal application", *Case Studies in Thermal Engineering*, **47**, pp. 103058 (2023). https://doi.org/10.1016/j.csite.2023.103058

33. Kai, Y., Ali, K., Ahmad, S., et al. "A case study of different magnetic strength fields and thermal energy effects in vortex generation of Ag-TiO2 hybrid nanofluid flow", *Case Studies in Thermal Engineering*, **47**, pp. 103115 (2023). https://doi.org/10.1016/j.csite.2023.103115

34. Hanif, H., Jamshed, W., Eid, M. R., et al. "Numerical Crank-Nicolson methodology analysis for hybridity aluminium alloy nanofluid flowing based-water via stretchable horizontal plate with thermal resistive effect", *Case Studies in Thermal Engineering*, **42**, pp. 102707 (2023). https://doi.org/10.1016/j.csite.2023.102707

35. Kai, Y., Ahmad, S., Takana, H., et al. "Thermal case study and generated vortices by dipole magnetic field in hybridized nanofluid flowing: Alternating direction implicit solution", *Results in Physics*, **49**, pp. 106464 (2023). https://doi.org/10.1016/j.rinp.2023.106464

36. Akolade, M. T., & Tijani, Y. O. "A comparative study of three dimensional flow of Casson–Williamson nanofluids past a riga plate: Spectral quasi-linearization approach", *Partial differential equations in applied mathematics*, **4**, pp. 100108 (2021). https://doi.org/10.1016/j.padiff.2021.100108

37. Mustafa, M., Hayat, T., Ioan, P., et al. "Stagnation-point flow and heat transfer of a Casson fluid towards a stretching sheet", *Zeitschrift für Naturforschung A*, **67**(1-2), pp. 70-76 (2012). https://doi.org/10.5560/zna.2011-0057

38. Nadeem, S., Haq, R. U., Akbar, N. S., et al. "MHD three-dimensional Casson fluid flow past a porous linearly stretching sheet", *Alexandria Engineering Journal*, **52**(4), pp. 577-582 (2013). https://doi.org/10.1016/j.aej.2013.08.005

39. Mahanta, G., & Shaw, S. "3D Casson fluid flow past a porous linearly stretching sheet with convective boundary condition", *Alexandria Engineering Journal*, **54**(3), pp. 653-659 (2015). https://doi.org/10.1016/j.aej.2015.04.014

40. Oyelakin, I. S., Mondal, S., & Sibanda, P. "Unsteady Casson nanofluid flow over a stretching sheet with thermal radiation, convective and slip boundary conditions", *Alexandria engineering journal*, **55**(2), pp. 1025-1035 (2016). https://doi.org/10.1016/j.aej.2016.03.003

41. Shah, Z., Gul, T., Khan, A. M., et al. "Effects of hall current on steady three dimensional non-newtonian nanofluid in a rotating frame with brownian motion and thermophoresis effects", *J. Eng. Technol*, **6**(280), pp. e296 (2017).

42. Anwar, M. I., Tanveer, N., Salleh, M. Z., et al. "Diffusive effects on hydrodynamic Casson nanofluid boundary layer flow over a stretching surface", *In Journal of*

Physics: Conference Series (Vol. 890, No. 1, p. 012047). IOP Publishing pp. (2017, September). 10.1088/1742-6596/890/1/012047

43. Hussanan, A., Salleh, M. Z., Khan, I., et al. "Analytical solution for suction and injection flow of a viscoplastic Casson fluid past a stretching surface in the presence of viscous dissipation", *Neural computing and applications*, **29**, pp. 1507-1515 (2018). https://doi.org/10.1007/s00521-016-2674-0

44. Mabood, F., & Das, K. "Outlining the impact of melting on MHD Casson fluid flow past a stretching sheet in a porous medium with radiation", *Heliyon*, **5**(2), pp. e01216 (2019). https://doi.org/10.1016/j.heliyon.2019.e01216

45. Ullah, I., Ali, F., Isa, S. M., et al. "Electro-magnetic radiative flowing of Williamson-dusty nanofluid along elongating sheet: Nanotechnology application", *Arabian Journal of Chemistry*, **16**(5), pp. 104698 (2023). https://doi.org/10.1016/j.arabjc.2023.104698

46. Khan, M. N., Ahmed, A., Ahammad, N. A., et al. "Insights into 3D flow of Casson fluid on exponential stretchable surface in rotating frame through porous medium", *Ain Shams Engineering Journal*, **14**(2), pp. 101849 (2023). https://doi.org/10.1016/j.asej.2022.101849

47. Lone, S. A., Raizah, Z., Shah, M. H., et al. "Thermal and Solutal Slips Impact on 3D-Biconvection Flow of Linearly Stratified Casson Nanofluid (Magnesium-Blood) Passed over a Bi-Stretching Surface in a Rotating Frame", *Results in Physics*, pp. 107139 (2023). https://doi.org/10.1016/j.rinp.2023.107139

48. Shah, Z., Dawar, A., Khan, I., et al. "Cattaneo-Christov model for electrical magnetite micropoler Casson ferrofluid over a stretching/shrinking sheet using effective thermal conductivity model", *Case Studies in Thermal Engineering*, **13**, pp. 100352 (2019). https://doi.org/10.1016/j.csite.2018.11.003

49. Gangaiah, T., Saidulu, N., & Venkata Lakshmi, A. "The Influence of Thermal Radiation on Mixed Convection MHD Flow of a Casson Nanofluid over an Exponentially Stretching Sheet", *International Journal of Nanoscience and Nanotechnology*, **15**(2), pp. 83-98 (2019).

50. Rafique, K., Imran Anwar, M., Misiran, et al. "Keller-box analysis of Buongiorno model with Brownian and thermophoretic diffusion for Casson nanofluid over an

inclined surface", *Symmetry*, **11**(11), pp. 1370 (2019). https://doi.org/10.3390/sym11111370

51. Ragupathi, P., Saranya, S., Mittal, H. V. R., et al. "Computational study on three-dimensional convective Casson nanofluid flow past a stretching sheet with Arrhenius activation energy and exponential heat source effects", *Complexity*, 2021, pp. 1-16 (2021). https://doi.org/10.1155/2021/5058751

52. Puneeth, V., Manjunatha, S., Madhukesh, J. K., et al. "Three-dimensional mixed convection flow of hybrid casson nanofluid past a non-linear stretching surface: A modified Buongiorno's model aspects", *Chaos, Solitons & Fractals*, **152**, pp. 111428 (2021). https://doi.org/10.1016/j.chaos.2021.111428

53. Al-Mamun, A., Arifuzzaman, S. M., Reza-E-Rabbi, S., et al. "Numerical simulation of periodic MHD casson nanofluid flow through porous stretching sheet", *SN Applied Sciences*, **3**(2), pp. 271 (2021). https://doi.org/10.1007/s42452-021-04140-3

54. Gangadhar, K., Edukondala Nayak, R., & Venkata Subba Rao, M. "Buoyancy effect on mixed convection boundary layer flow of Casson fluid over a non linear stretched sheet using the spectral relaxation method", *International Journal of Ambient Energy*, **43**(1), pp. 1994-2002 (2022). https://doi.org/10.1080/01430750.2020.1722963

55. Garoosi, F., Jahanshaloo, L., Rashidi, M. M., et al. "Numerical simulation of natural convection of the nanofluid in heat exchangers using a Buongiorno model", *Applied Mathematics and Computation*, **254**, pp. 183-203 (2015). https://doi.org/10.1016/j.amc.2014.12.116

56. Turkyilmazoglu, M. "On the transparent effects of Buongiorno nanofluid model on heat and mass transfer", *The European Physical Journal Plus*, **136**(4), pp. 1-15 (2021). https://doi.org/10.1140/epjp/s13360-021-01359-2

57. Akbar, S., & Sohail, M. "Three dimensional MHD viscous flow under the influence of thermal radiation and viscous dissipation", *International Journal of Emerging Multidisciplinaries: Mathematics*, **1**(3), pp. 106-117 (2022). https://doi.org/10.54938/ijemdm.2022.01.3.122

58. Li, S., Akbar, S., Sohail, M., et al. "Influence of buoyancy and viscous dissipation effects on 3D magneto hydrodynamic viscous hybrid nano fluid (MgO− TiO2)

under slip conditions", *Case Studies in Thermal Engineering*, **49**, pp. 103281 (2023). https://doi.org/10.1016/j.csite.2023.103281

59. Nazir, U., Sohail, M., Mukdasai, K., et al. "Applications of variable thermal properties in Carreau material with ion slip and Hall forces towards cone using a non-Fourier approach via FE-method and mesh-free study", *Frontiers in Materials*, **9**, pp. 1054138 (2022). https://doi.org/10.3389/fmats.2022.1054138

60. Zhang, X., Yang, D., Katbar, N. M., et al. "Entropy and thermal case description of monophase magneto nanofluid with thermal jump and Ohmic heating employing finite element methodology", *Case Studies in Thermal Engineering*, **45**, pp. 102919 (2023). https://doi.org/10.1016/j.csite.2023.102919

61. Jamshed, W., Nisar, K. S., Gowda, R. P., et al. "Radiative heat transfer of second grade nanofluid flow past a porous flat surface: a single-phase mathematical model", *Physica Scripta*, **96**(6), pp. 064006 (2021). 10.1088/1402-4896/abf57d

62. Jamshed, W., Devi, S. U., & Nisar, K. S. "Single phase based study of Ag-Cu/EO Williamson hybrid nanofluid flow over a stretching surface with shape factor", *Physica Scripta*, **96**(6), pp. 065202 (2021). 10.1088/1402-4896/abecc0

63. Ahmad, I., Qureshi, N., Al-Khaled, K., et al. "Magnetohydrodynamic time dependent 3-D simulations for Casson nano-material configured by unsteady stretched surface with thermal radiation and chemical reaction aspects", *Journal of Nanofluids*, **10**(2), pp. 232-245 (2021). https://doi.org/10.1166/jon.2021.1779

64. Haider, A., Ayub, A., Madassar, N., et al. "Energy transference in time- dependent Cattaneo–Christov double diffusion of second- grade fluid with variable thermal conductivity", *Heat Transfer*, **50**(8), pp. 8224-8242 (2021). https://doi.org/10.1002/htj.22274

65. Rasool, G., Shah, S. Z. H., Sajid, T., et al. "Spectral Relaxation methodology for chemical and bioconvection processes for cross nanofluid flowing around an oblique cylinder with a slanted magnetic field effect", *Coatings*, **12**(10), pp. 1560 (2022). https://doi.org/10.3390/coatings12101560

66. Farooq, U., Waqas, H., Alhazmi, S. E., et al. "Numerical treatment of casson nanofluid bioconvectional flow with heat transfer due to stretching cylinder/plate:

Variable physical properties", *Arabian Journal of Chemistry*, **16**(4), pp. 104589 (2023). https://doi.org/10.1016/j.arabjc.2023.104589

67. Kumaraswamy Naidu, K., Harish Babu, D., & Satya Narayana, P. V. "Bioconvection in magneto hydrodynamics Casson nanoliquid (Fe3O4-sodium alginate) With gyrotactic microorganisms over an exponential stretching sheet", *Journal of Nanofluids*, **10**(3), pp. 327-338 (2021). https://doi.org/10.1166/jon.2021.1789

68. Tawade, J. V., Guled, C. N., Noeiaghdam, S., et al. "Effects of thermophoresis and Brownian motion for thermal and chemically reacting Casson nanofluid flow over a linearly stretching sheet", *Results in Engineering*, **15**, pp. 100448 (2022). https://doi.org/10.1016/j.rineng.2022.100448

69. Botmart, T., Shah, S. Z. H., Sabir, Z., et al. "The inclination of magnetic dipole effect and nanoscale exchange of heat of the Cross nanofluid", *Waves in Random and Complex Media*, pp. 1-16 (2022). https://doi.org/10.1080/17455030.2022.2128225

70. Darvesh, A., Sajid, T., Jamshed, W., et al. "Rheology of variable viscosity-based mixed convective inclined magnetized cross nanofluid with varying thermal conductivity", *Applied Sciences*, **12**(18), pp. 9041 (2022). https://doi.org/10.3390/app12189041

71. Al-Kouz, W., & Owhaib, W. "Numerical analysis of Casson nanofluid three-dimensional flow over a rotating frame exposed to a prescribed heat flux with viscous heating", *Scientific Reports*, **12**(1), pp. 4256 (2022). https://doi.org/10.1038/s41598-022-08211-2

Dr. MUHAMMAD SOHAIL belongs to a very small village of district Haripur, Khyber Pakhtunkhwa, Pakistan. He got his PhD Mathematics degree from the Institute of Space Technology Islamabad, Pakistan in 2020. Currently, he is working as an Assistant Professor Mathematicsat Khwaja Fareed University of Engineering and Information Technology Rahim Yar Khan, Pakistan. His research interests are on CFD simulation, mass transport, heat transfer, mathematical modelling, nonlinear dynamics, stability analysis, numerical and analytical methods, fractional differential equations, mixed convection and heat exchangers. He has published more than about 140 research articles in different peer reviewed international journals.

Syed Qasim Hussain Shah has completed MS Mathematics from Khwaja Fareed University of Engineering and Information Technology Rahim Yar Khan, Pakistan and his interest is in fluid mechanics.

Faisal Sultan is working as an Assistant Professor Mathematics and Head of Department at Khwaja Fareed University of Engineering and Information Technology Rahim Yar Khan, Pakistan.

Shah Jahan is working as an Assistant Professor Mathematics at Khwaja Fareed University of Engineering and Information Technology Rahim Yar Khan, Pakistan.

Syed Tehseen Abbas has completed MS Mathematics under the supervision of Dr. Muhammad Sohail from Khwaja Fareed University of Engineering and Information Technology Rahim Yar Khan, Pakistan and his interest is in applied mathematics and in fluid mechanics.

Figures and Tables Captions.

Fig. 1. The problem under examination is depicted in a schematic diagram.

Fig. 2. Pictorial presentation of used scheme.

Fig. 3. β impact on $f'(\eta)$ for the values $S = 0.8$; $Ec = 0.2$; $\alpha = 0.8$; $M = 0.0$; $P_r = 1.0$; $Nt = 0.2$; $Ro = 0.1$; $Lb = 0.5$; $Le = 0.2$; $Nb = 0.1$; $Pe = 1.0$; $\delta_1 = 0.0$.

Fig. 4. Ro impact on $f'(\eta)$ for the values $S = 0.8$; $\alpha = 0.8$; $M = 0.0$; $\beta = 1.0$; $Ec = 0.2$; $Lb = 0.5$; $Le = 0.2$; $Nt = 0.2$; $P_r = 1.0$; $Nb = 0.1$; $Pe = 1.0$; $\delta_1 = 0.0$.

Fig. 5. M impact on $f'(\eta)$ for the values $S = 0.8$; $\alpha = 0.8$; $Ro = 0.1$; $Ec = 0.2$; $\beta = 1.0$; $Nb = 0.1$; $Lb = 0.5$; $Le = 0.2$; $P_r = 1.0$; $Nt = 0.2$; $Pe = 1.0$; $\delta_1 = 0.0$.

Fig. 6. β impact on $g'(\eta)$ for the values $S = 0.8$; $Ec = 0.2$; $M = 0.0$; $Nb = 0.1$; $Nt = 0.2$; $Pe = 1.0$; $\delta_1 = 0.0$, $\alpha = 0.8$; $P_r = 1.0$; $Ro = 0.1$; $Lb = 0.5$; $Le = 0.2$.

Fig. 7. Ro impact on $g'(\eta)$ for the values $S = 0.8$; $Ec = 0.2$; $M = 0.0$; $Lb = 0.5$; $Nt = 0.2$; $Le = 0.2$; $\alpha = 0.8$; $\beta = 1.0$; $P_r = 1.0$; $Nb = 0.1$; $Pe = 1.0$; $\delta_1 = 0.0$.

Fig. 8. M impact on $g'(\eta)$ for the values $S = 0.8$; $\alpha = 0.8$; $Ec = 0.2$; $\beta = 1.0$; $Nt = 0.2$; $Lb = 0.5$; $Le = 0.2$; $P_r = 1.0$; $Ro = 0.1$; $Nb = 0.1$; $Pe = 1.0$; $\delta_1 = 0.0$.

Fig. 9. P_r impact on $\theta(\eta)$ for the values $S = 0.8$; $Nb = 0.1$; $Ro = 0.1$; $Ec = 0.2$; $Lb = 0.5$; $Le = 0.2$; $M = 0.0$; $\alpha = 0.8$; $\beta = 1.0$; $Nt = 0.2$; $Pe = 1.0$; $\delta_1 = 0.0$.

Fig. 10. Nb impact on $\theta(\eta)$ for the values $S = 0.8$; $\alpha = 0.8$; $Le = 0.2$; $Ec = 0.2$; $P_r = 1.0$; $Nt = 0.2$; $M = 0.0$; $\beta = 1.0$; $Ro = 0.1$; $Lb = 0.5$; $Pe = 1.0$; $\delta_1 = 0.0$.

Fig. 11. Nt impact on $\theta(\eta)$ for the values $S = 0.8$; $Le = 0.2$; $M = 0.0$; $Ec = 0.2$; $P_r = 1.0$; $Pe = 1.0$; $\delta_1 = 0.0$, $Nb = 0.1$; $\alpha = 0.8$; $\beta = 1.0$; $Ro = 0.1$; $Lb = 0.5$.

Fig. 12. Ec impact on $\theta(\eta)$ for the values $S = 0.8$; $\alpha = 0.8$; $\beta = 1.0$; $Le = 0.2$; $M = 0.0$; $P_r = 1.0$; $Nb = 0.1$; $Nt = 0.2$; $Ro = 0.1$; $Lb = 0.5$; $Pe = 1.0$; $\delta_1 = 0.0$.

Fig. 13. β impact on $\theta(\eta)$ for the values $S = 0.8$; $Ec = 0.2$; $M = 0.0$; $P_r = 1.0$; $Nb = 0.1$; $Nt = 0.2$; $\alpha = 0.8$; $Ro = 0.1$; $Lb = 0.5$; $Le = 0.2$; $Pe = 1.0$; $\delta_1 = 0.0$.

Fig. 14. Nt impact on $\varphi(\eta)$ for the values $S = 0.8$; $\alpha = 0.8$; $Ro = 0.1$; $Lb = 0.5$; $Le = 0.2$; $M = 0.0$; $Ec = 0.2$; $\beta = 1.0$; $P_r = 1.0$; $Nb = 0.1$; $Pe = 1.0$; $\delta_1 = 0.0$.

Fig. 15. Nb impact on $\varphi(\eta)$ for the values $S = 0.8$; $\alpha = 0.8$; $Ro = 0.1$; $Lb = 0.5$; $Le = 0.2$; $M = 0.0$; $Ec = 0.2$; $\beta = 1.0$; $P_r = 1.0$; $Nt = 0.2$; $Pe = 1.0$; $\delta_1 = 0.0$.

Fig. 16. Le impact on $\varphi(\eta)$ for the values $S = 0.8$; $\alpha = 0.8$; $\beta = 1.0$; $P_r = 1.0$; $Nt = 0.2$; $Pe = 1.0$; $Nb = 0.1$; $Ec = 0.2$; $Ro = 0.1$; $Lb = 0.5$; $M = 0.0$; $\delta_1 = 0.0$.

Fig. 17. Lb impact on $\chi(\eta)$ for the values $S = 0.8$; $\alpha = 0.8$; $P_r = 1.0$; $Nt = 0.2$; $Pe = 1.0$; $Nb = 0.1$; $\delta_1 = 0.0$, $Ec = 0.2$; $Ro = 0.1$; $Le = 0.2$; $M = 0.0$; $\beta = 1.0$.

Fig. 18. Pe impact on $\chi(\eta)$ for the values $S = 0.8$; $\alpha = 0.8$; $Ec = 0.2$; $Ro = 0.1$; $M = 0.0$; $Le = 0.2$; $Nb = 0.1$; $\beta = 1.0$; $P_r = 1.0$; $Nt = 0.2$; $Lb = 0.5$; $\delta_1 = 0.0$.

Fig. 19. δ_1 impact on $\chi(\eta)$ for the values $S = 0.8$; $Ro = 0.1$; $Le = 0.2$; $M = 0.0$; $P_r = 1.0$; $Nt = 0.2$; $Lb = 0.5$; $\alpha = 0.8$; $Ec = 0.2$; $\beta = 1.0$; $Nb = 0.1$; $Pe = 1.0$.

Table 1. Numerical Outcomes $Nb = 0.1$ and $Nt = 0.05$.

$$u \to 0,\ v \to 0, \qquad w \to 0,\ T \to T_\infty, n \to n_\infty, \qquad C \to C_\infty \ \text{when}\ z \to \infty$$

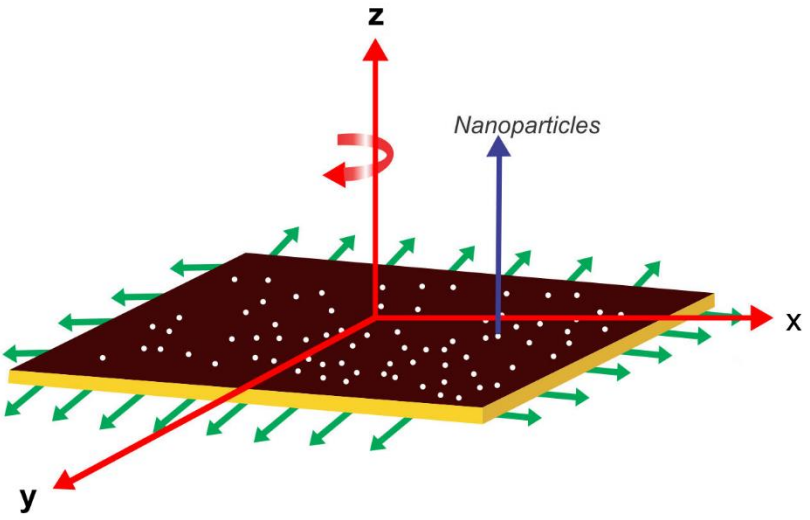

$$u = u_w(x) = ax, v = v_w(y) = by, w = w, T = T_w, C = C_w, n = n_w \ \text{at}\ z = 0$$

Fig. 1. The problem under examination is depicted in a schematic diagram.

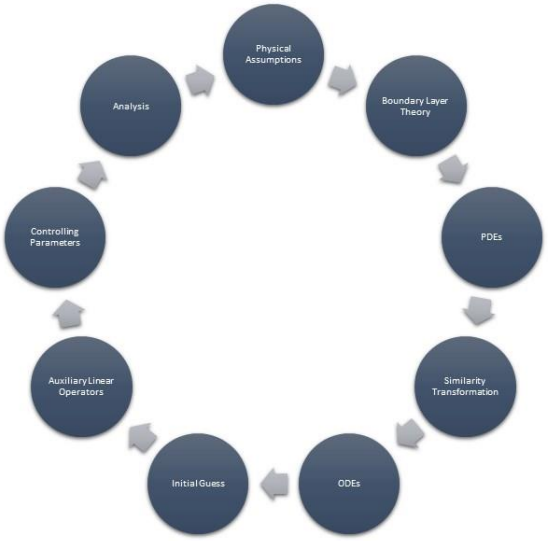

Fig. 2. Pictorial presentation of used scheme.

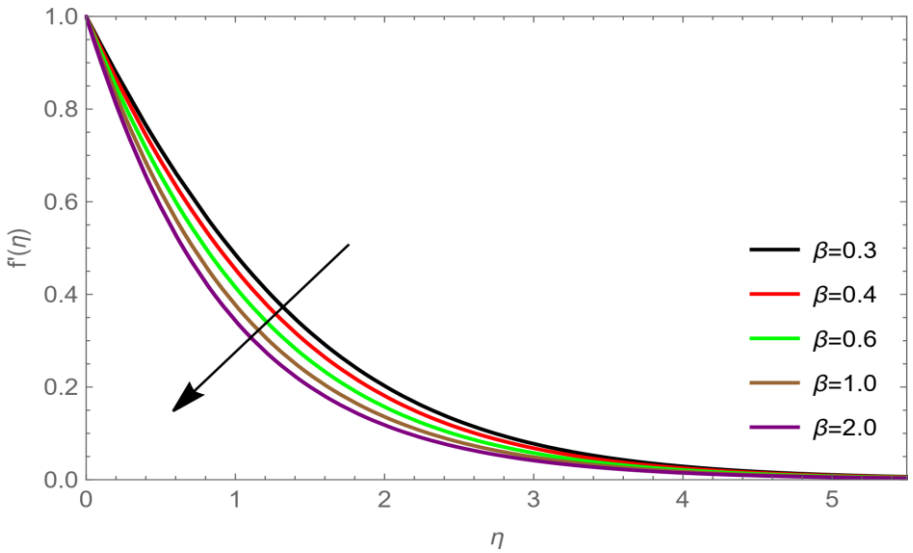

Fig. 3. β impact on $f'(\eta)$ for the values $S = 0.8$; $Ec = 0.2$; $\alpha = 0.8$; $M = 0.0$; $P_r = 1.0$; $Nt = 0.2$; $Ro = 0.1$; $Lb = 0.5$; $Le = 0.2$; $Nb = 0.1$; $Pe = 1.0$; $\delta_1 = 0.0$.

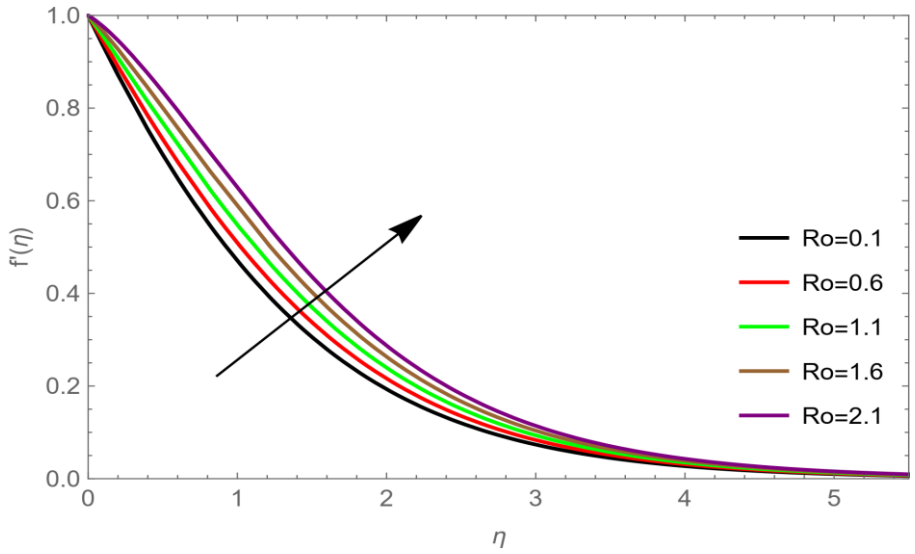

Fig. 4. *Ro* impact on $f'(\eta)$ for the values $S = 0.8$; $\alpha = 0.8$; $M = 0.0$; $\beta = 1.0$; $Ec = 0.2$; $Lb = 0.5$; $Le = 0.2$; $Nt = 0.2$; $P_r = 1.0$; $Nb = 0.1$; $Pe = 1.0$; $\delta_1 = 0.0$.

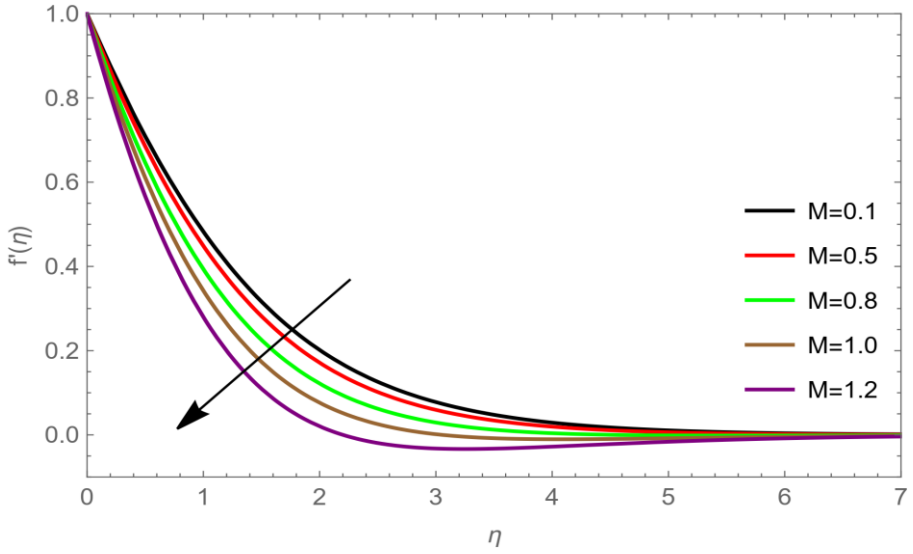

Fig. 5. M impact on $f'(\eta)$ for the values $S = 0.8$; $\alpha = 0.8$; $Ro = 0.1$; $Ec = 0.2$; $\beta = 1.0$; $Nb = 0.1$; $Lb = 0.5$; $Le = 0.2$; $P_r = 1.0$; $Nt = 0.2$; $Pe = 1.0$; $\delta_1 = 0.0$.

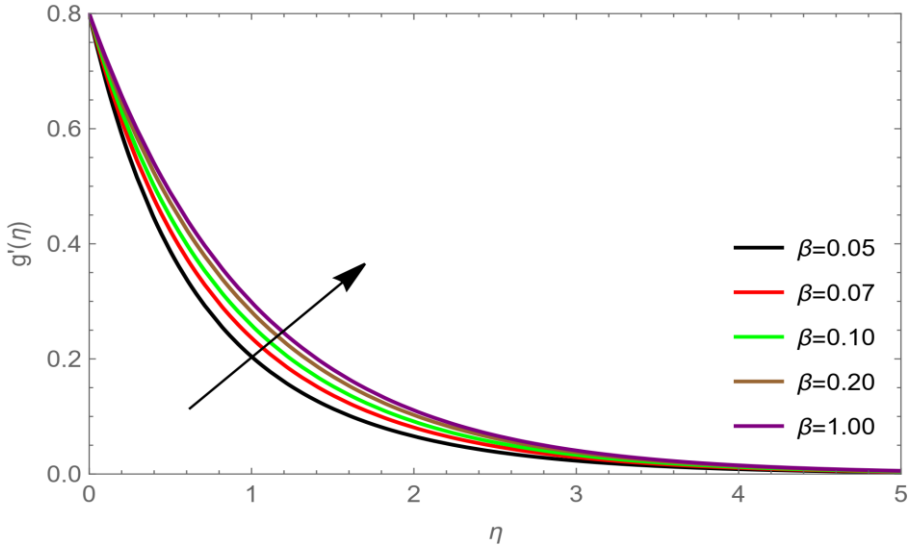

Fig. 6. β impact on $g'(\eta)$ for the values $S = 0.8$; $Ec = 0.2$; $M = 0.0$; $Nb =$

0.1; $Nt = 0.2$; $Pe = 1.0$; $\delta_1 = 0.0$, $\alpha = 0.8$; $P_r = 1.0$; $Ro = 0.1$; $Lb = 0.5$; $Le = 0.2$.

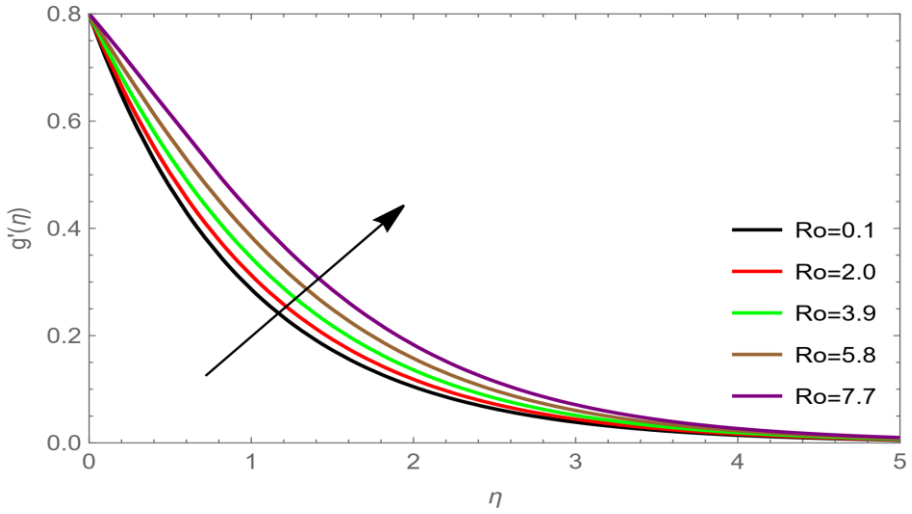

Fig. 7. Ro impact on $g'(\eta)$ for the values $S = 0.8$; $Ec = 0.2$; $M = 0.0$; $Lb = 0.5$; $Nt = 0.2$; $Le = 0.2$; $\alpha = 0.8$; $\beta = 1.0$; $P_r = 1.0$; $Nb = 0.1$; $Pe = 1.0$; $\delta_1 = 0.0$.

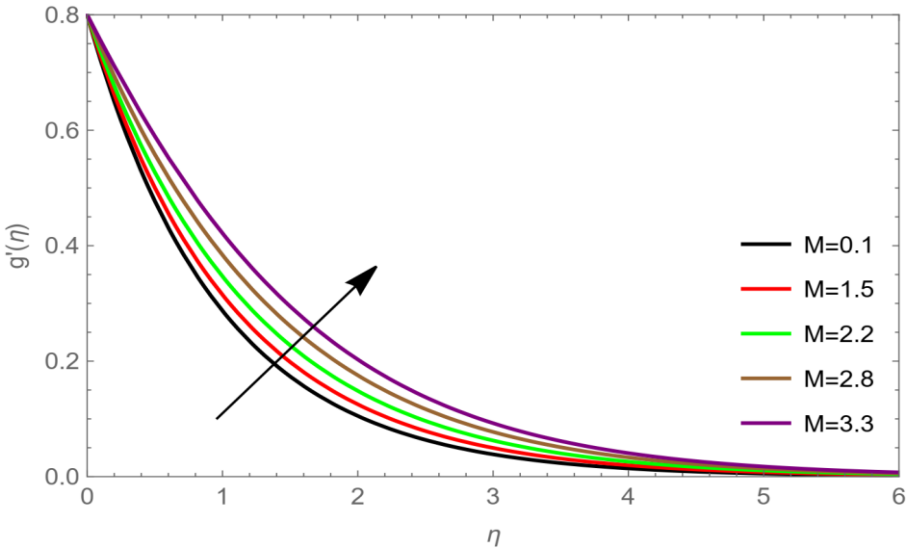

Fig. 8. M impact on $g'(\eta)$ for the values $S = 0.8$; $\alpha = 0.8$; $Ec = 0.2$; $\beta = 1.0$; $Nt = 0.2$; $Lb = 0.5$; $Le = 0.2$; $P_r = 1.0$; $Ro = 0.1$; $Nb = 0.1$; $Pe = 1.0$; $\delta_1 = 0.0$.

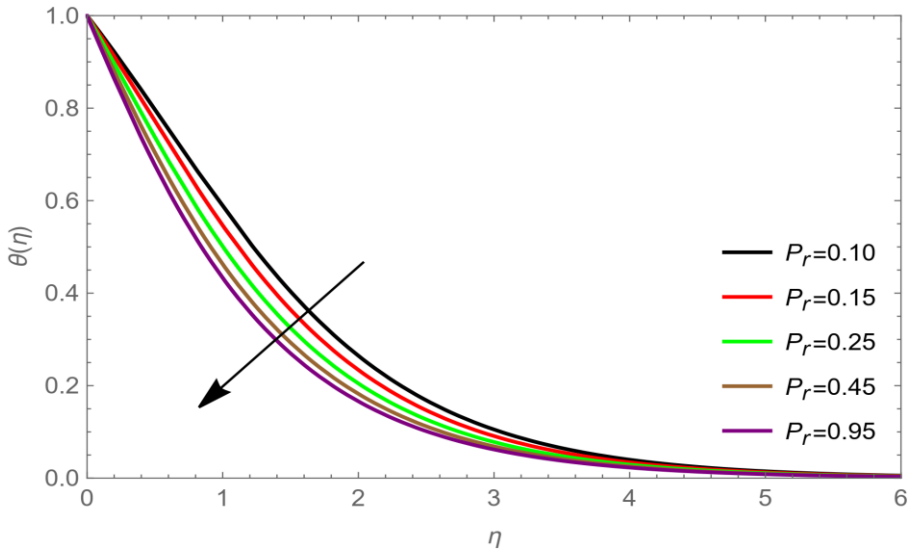

Fig. 9. P_r impact on $\theta(\eta)$ for the values $S = 0.8$; $Nb = 0.1$; $Ro = 0.1$; $Ec = 0.2$; $Lb = 0.5$; $Le = 0.2$; $M = 0.0$; $\alpha = 0.8$; $\beta = 1.0$; $Nt = 0.2$; $Pe = 1.0$; $\delta_1 = 0.0$.

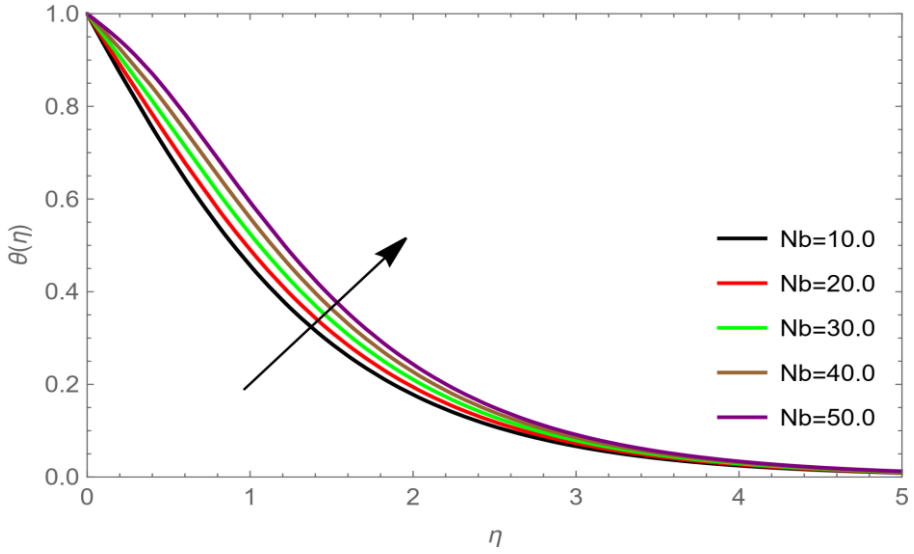

Fig. 10. Nb impact on $\theta(\eta)$ for the values $S = 0.8$; $\alpha = 0.8$; $Le = 0.2$; $Ec = 0.2$; $P_r = 1.0$; $Nt = 0.2$; $M = 0.0$; $\beta = 1.0$; $Ro = 0.1$; $Lb = 0.5$; $Pe = 1.0$; $\delta_1 = 0.0$.

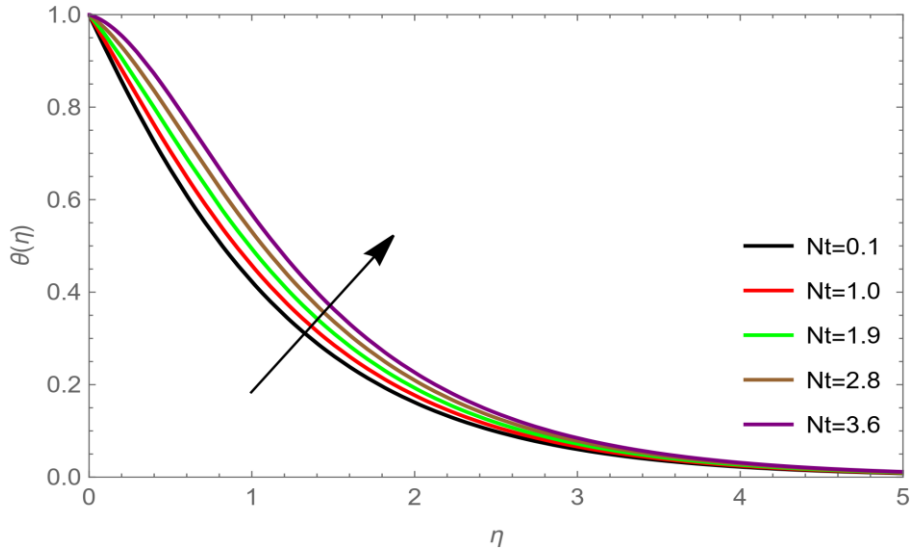

Fig. 11. Nt impact on $\theta(\eta)$ for the values $S = 0.8$; $Le = 0.2$; $M = 0.0$; $Ec =$

0.2; $P_r = 1.0$; $Pe = 1.0$; $\delta_1 = 0.0$, $Nb = 0.1$; $\alpha = 0.8$; $\beta = 1.0$; $Ro = 0.1$; $Lb = 0.5$.

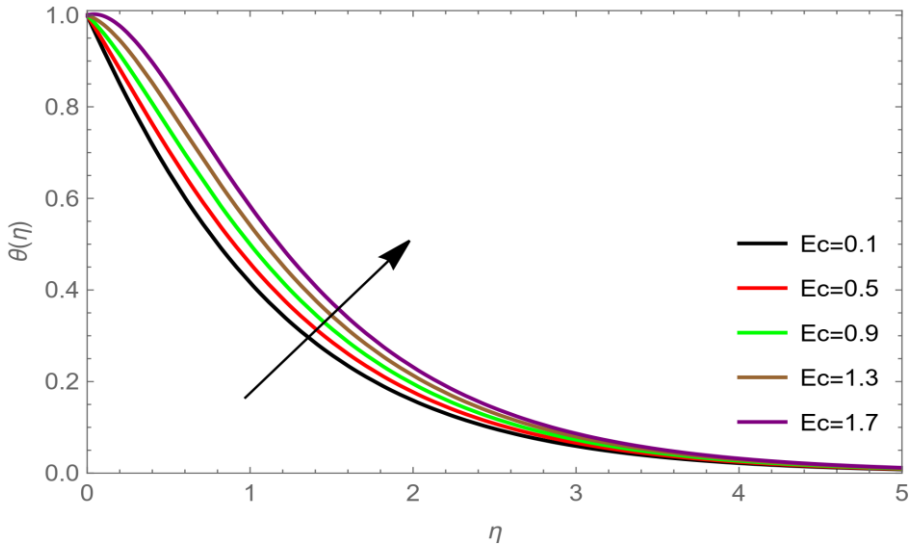

Fig. 12. Ec impact on $\theta(\eta)$ for the values $S = 0.8$; $\alpha = 0.8$; $\beta = 1.0$; $Le = 0.2$; $M = 0.0$; $P_r = 1.0$; $Nb = 0.1$; $Nt = 0.2$; $Ro = 0.1$; $Lb = 0.5$; $Pe = 1.0$; $\delta_1 = 0.0$.

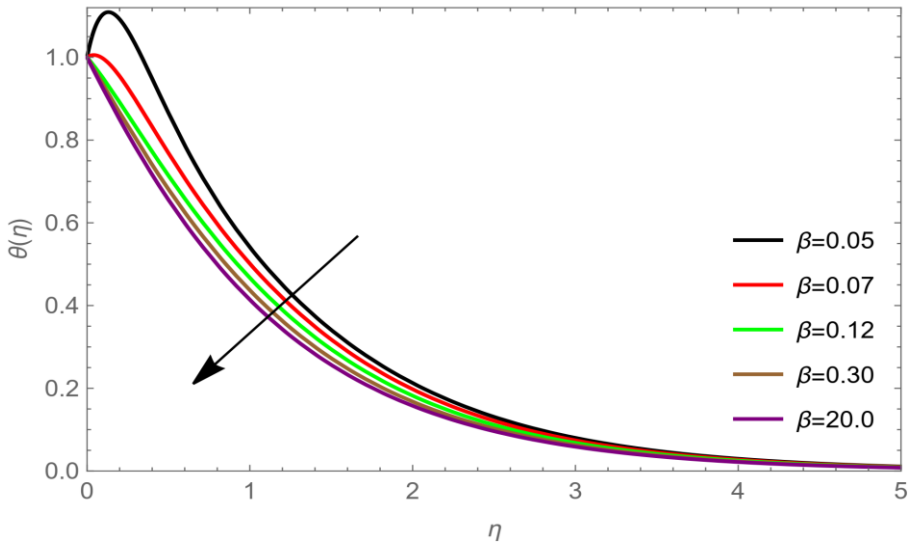

Fig. 13. β impact on $\theta(\eta)$ for the values $S = 0.8$; $Ec = 0.2$; $M = 0.0$; $P_r = 1.0$; $Nb = 0.1$; $Nt = 0.2$; $\alpha = 0.8$; $Ro = 0.1$; $Lb = 0.5$; $Le = 0.2$; $Pe = 1.0$; $\delta_1 = 0.0$.

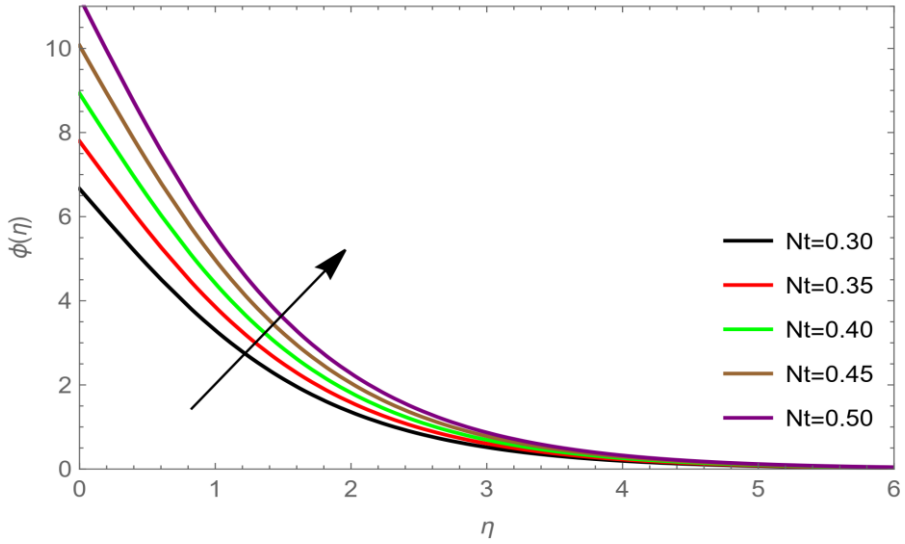

Fig. 14. Nt impact on $\varphi(\eta)$ for the values $S = 0.8$; $\alpha = 0.8$; $Ro = 0.1$; $Lb =$

0.5; $Le = 0.2$; $M = 0.0$; $Ec = 0.2$; $\beta = 1.0$; $P_r = 1.0$; $Nb = 0.1$; $Pe = 1.0$; $\delta_1 = 0.0$.

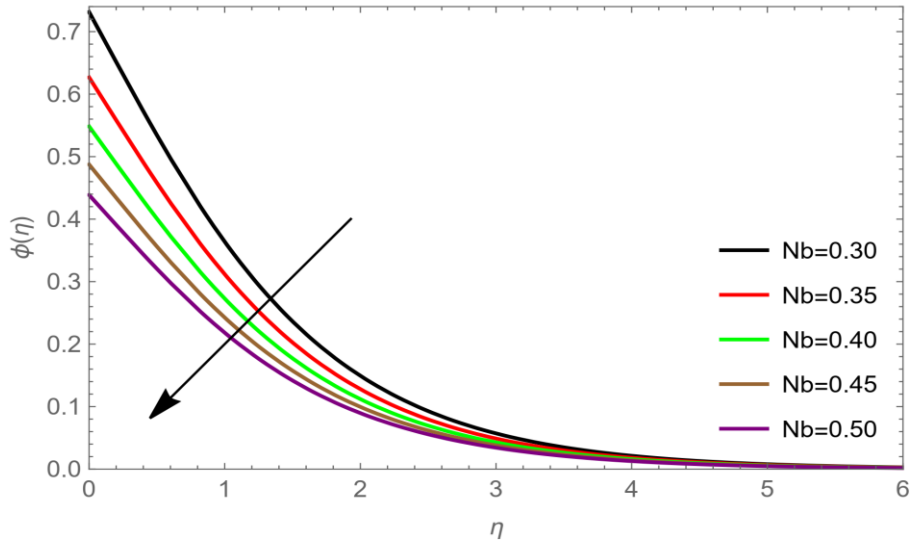

Fig. 15. Nb impact on $\varphi(\eta)$ for the values $S = 0.8$; $\alpha = 0.8$; $Ro = 0.1$; $Lb = 0.5$; $Le = 0.2$; $M = 0.0$; $Ec = 0.2$; $\beta = 1.0$; $P_r = 1.0$; $Nt = 0.2$; $Pe = 1.0$; $\delta_1 = 0.0$.

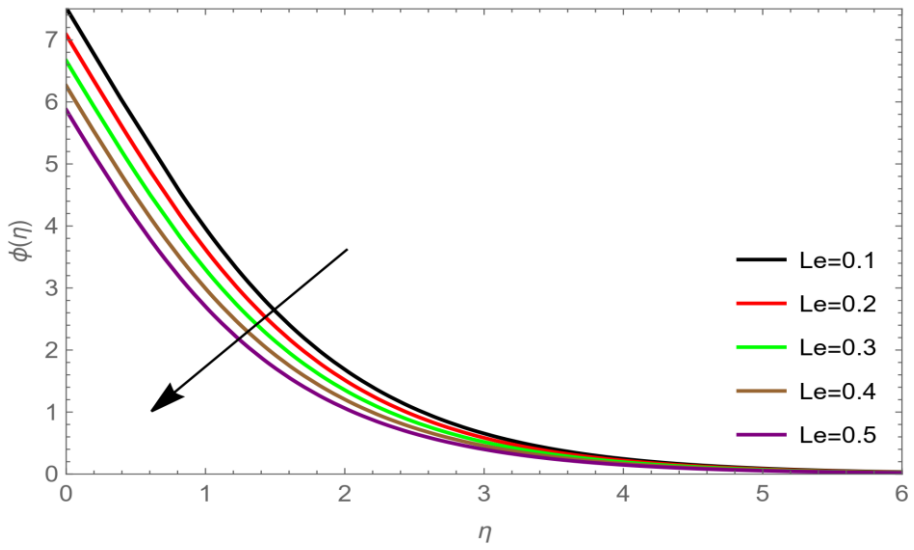

Fig. 16. *Le* impact on $\varphi(\eta)$ for the values $S = 0.8$; $\alpha = 0.8$; $\beta = 1.0$; $P_r = 1.0$; $Nt = 0.2$; $Pe = 1.0$; $Nb = 0.1$; $Ec = 0.2$; $Ro = 0.1$; $Lb = 0.5$; $M = 0.0$; $\delta_1 = 0.0$.

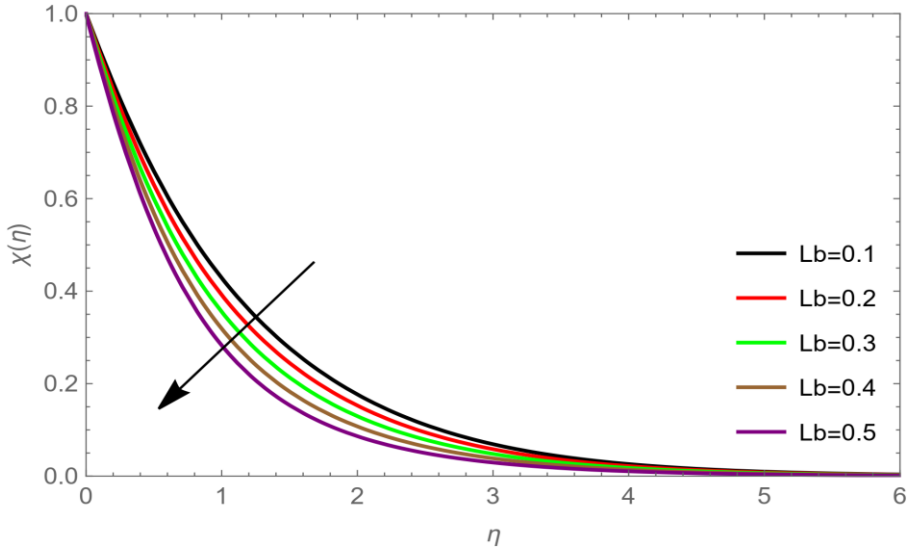

Fig. 17. *Lb* impact on $\chi(\eta)$ for the values $S = 0.8$; $\alpha = 0.8$; $P_r = 1.0$; $Nt =$

$0.2;\ Pe\ = 1.0;\ \ Nb\ = 0.1;\ \ \delta_1\ = 0.0,\ Ec\ = 0.2;\ Ro\ = 0.1;\ Le\ = 0.2;\ \ M\ =$

$0.0;\ \beta\ = 1.0.$

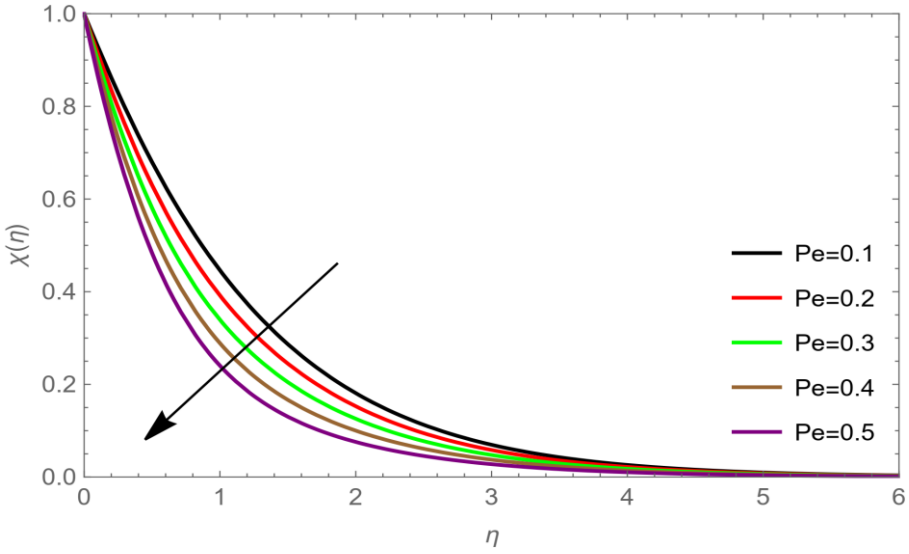

Fig. 18. Pe impact on $\chi(\eta)$ for the values $S\ = 0.8;\ \alpha\ = 0.8;\ Ec\ = 0.2;\ Ro\ =$ $0.1;\ M\ = 0.0;\ \ Le\ = 0.2;\ Nb\ = 0.1;\ \beta\ = 1.0;\ P_r\ = 1.0;\ Nt\ = 0.2;\ Lb\ = 0.5;\ \ \delta_1\ =$ $0.0.$

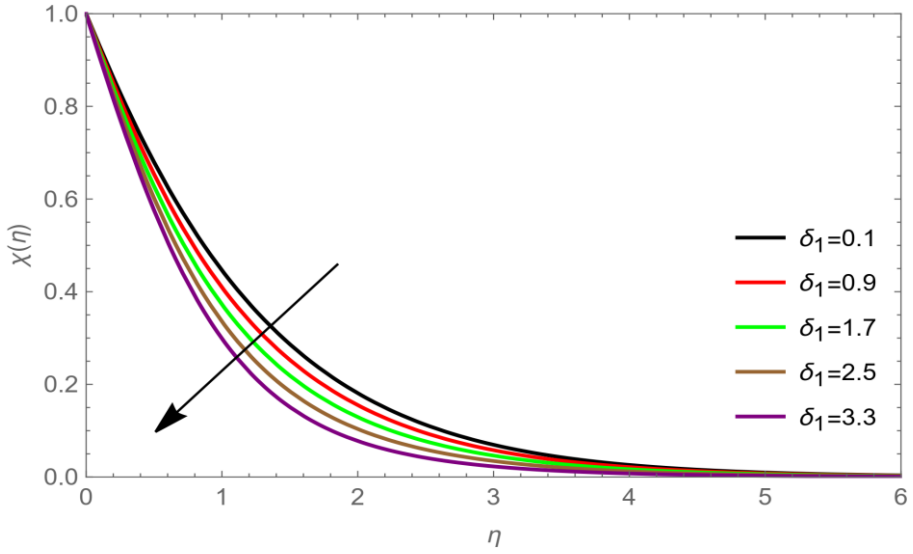

Fig. 19. δ_1 impact on $\chi(\eta)$ for the values $S = 0.8$; $Ro = 0.1$; $Le = 0.2$; $M = 0.0$; $P_r = 1.0$; $Nt = 0.2$; $Lb = 0.5$; $\alpha = 0.8$; $Ec = 0.2$; $\beta = 1.0$; $Nb = 0.1$; $Pe = 1.0$.

Table 1. Numerical Outcomes $Nb = 0.1$ and $Nt = 0.05$.

β	$\mathrm{Re}_x^{0.5} Sf_x$	$\mathrm{Re}_x^{0.5} Sf_y$	$\mathrm{Re}_x^{-0.5} Nu_x$	$\mathrm{Re}_x^{-0.5} Sh_x$
0.2	-4.319850835	-1.945788288	1.000000000	0.500000000
0.4	-3.563695142	-1.605193443	1.000000000	0.500000000
0.6	-3.325422742	-1.497868523	1.000000000	0.500000000
0.8	-3.239888144	-1.459341217	1.000000000	0.500000000